



HAL
open science

Self-oscillating polymer membranes with chemically fueled pore size oscillation mediated by pH-responsive polymer

Johanne Pirkin-Benameur, Denis Bouyer, Damien Quemener

► **To cite this version:**

Johanne Pirkin-Benameur, Denis Bouyer, Damien Quemener. Self-oscillating polymer membranes with chemically fueled pore size oscillation mediated by pH-responsive polymer. *Journal of Membrane Science*, 2022, 658, pp.120742. 10.1016/J.MEMSCI.2022.120742 . hal-03736421

HAL Id: hal-03736421

<https://hal.umontpellier.fr/hal-03736421>

Submitted on 4 Oct 2023

HAL is a multi-disciplinary open access archive for the deposit and dissemination of scientific research documents, whether they are published or not. The documents may come from teaching and research institutions in France or abroad, or from public or private research centers.

L'archive ouverte pluridisciplinaire **HAL**, est destinée au dépôt et à la diffusion de documents scientifiques de niveau recherche, publiés ou non, émanant des établissements d'enseignement et de recherche français ou étrangers, des laboratoires publics ou privés.

1 Self-oscillating polymer membranes with chemically fueled 2 pore size oscillation mediated by pH-responsive polymer

3
4 Johanne Pirkin-Benameur, Denis Bouyer, Damien Quemener*

5 Institut Européen des Membranes, IEM-UMR 5635, Univ Montpellier, ENSCM, CNRS,34090 Montpellier,
6 France.

7 *Corresponding author

8 Email address: damien.quemener@umontpellier.fr (D. Quémener)

9 10 Abstract

11
12 Soft-matter materials research has considerably evolved in the last decades, mainly by promoting responsive
13 polymer systems. Up to now, the dynamic behavior in materials was always reached by the action of an outside
14 trigger (pH, light, etc.). This constraint has been relieved in a new class of materials that experienced self-
15 oscillation. In this work, the self-regulating pH cycles caused by a chemical oscillator will induce autonomous
16 pH-sensible polymer chain movements at the membrane interface, causing continuous pore-size oscillation
17 cycles and thus a self-oscillating flux. This work involved the functionalisation of polyethersulfone commercial
18 membranes to achieve pore size oscillations. The pH-sensitive polymer, poly(methacrylic acid) (PMAA), was
19 obtained by deprotection of poly(tert-butyl methacrylate) (PtBuMA) synthesized by RAFT polymerization. To
20 adapt this functionalisation to all types of commercial membranes, a thin layer of polydopamine (PDA) was
21 deposited on the top of the membrane, which then allows a Michael-thiol-ene reaction between PDA and thiol-
22 functionalised PMAA, obtained from prior aminolysis of PtBuMA. The functionalisation steps were
23 characterized by XPS, SEM, water contact angle, and permeability measurements. Membranes were then placed
24 in a filtration system containing a chemical pH oscillator to control the PMAA chain conformation through the
25 pH cycle. Water permeation analysis showed a dependence between permeability and PMAA conformation,
26 leading to the conclusion that there is indeed a continuous oscillation in membrane pore size.

27 Keywords

28
29 Self-oscillating membrane; pH oscillator; stimuli-responsive membrane; polydopamine; pH-sensitive polymer

30
31

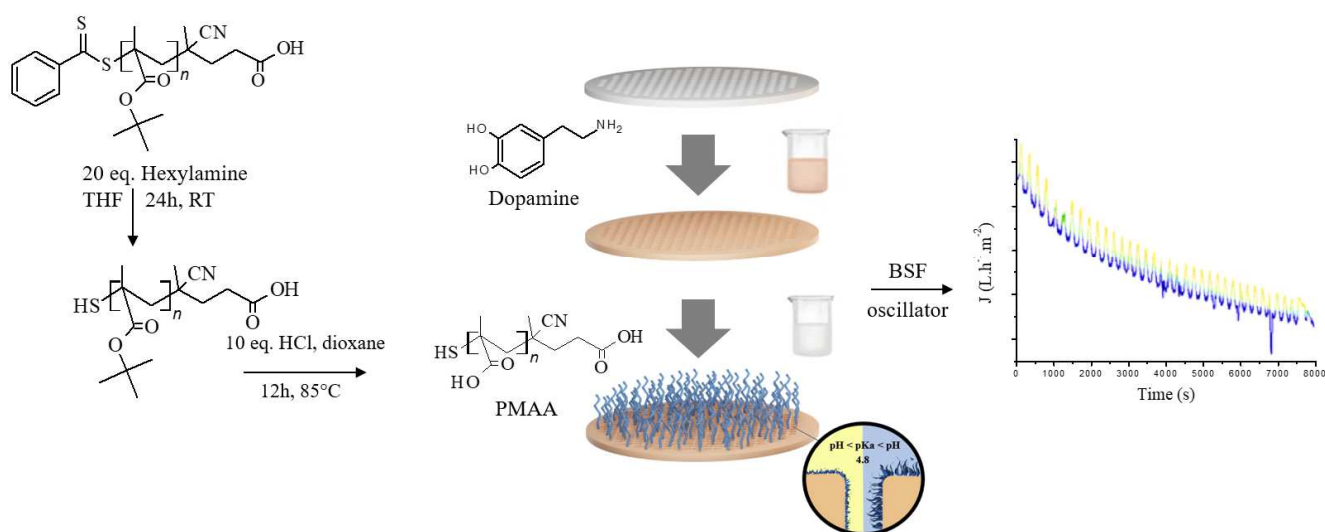
32 1. Introduction

33 Our century is filled with many issues, such as chemical pollution [1], which is partly caused by the lack of
34 responsiveness of current materials. This problem and resource shortages are forcing us to develop materials
35 with an improved lifespan, notably through new functionalities. Nature creates materials that meet this challenge,
36 because of their advanced compositions and functions. Thus, one of the major challenges in the materials field is
37 to reach the autonomy level of natural materials. Nowadays materials explored to mimic the nature include
38 stimuli-sensitive systems [2]. Several stimuli have been studied to that purpose such as temperature [3], pH [4],
39 mechanical strength [5], biological triggers [6], and electromagnetic fields [7] for applications such as
40 chromatography [8], surface functionalisation [9], and sensor [10]. pH being one of the most common variables
41 for biological reactions[11,12], pH sensitive polymers have found various applications, especially in biomedical
42 field [13]. pH-sensitive membranes have also been developed due to the potential brought by this trigger such as
43 stimuli-responsive permeation [14], pore size change [15,16], nanoparticle fractionation[17], or antifouling
44 properties [18]. The pH responsiveness was introduced either during the membrane formation [19–21] or via a
45 post functionalisation [17,18,22–24]. However, the limitation of these membranes, and materials in general, is
46 that they must be “manually” activated and deactivated by triggering the corresponding stimulus [25]. Materials
47 that cross this boundary gains autonomy, whether it is by allowing self-protection [26], self-reporting [27], self-
48 healing [28], regenerating [29], or controlled degradation ability [30].

49 A standalone promising feature in this category that has recently been reported is self-oscillation. It involves
50 coupling a sensitive material with a chemical oscillator. A chemical oscillator is a network of chemical reactions
51 in which the concentration of the products changes on a cyclic basis until the source of energy is exhausted.
52 When coupled to a material, continuous periodic variation of macroscopic properties such as its volume or its
53 hydrophobic-hydrophilic balance is observed. Since the first self-oscillating materials developed by Yoshida
54 [31], many works have been carried out with the Belousov-Zhabotinsky (BZ) oscillator, such as self-walking gel
55 [32], self-oscillating gel for mass transports [33], soft actuators of organized self-oscillating microgels [34] or
56 self-oscillating chemoelectrical interface of solution-gated ion-sensitive field-effect transistor [35]. This concept
57 doesn't allow only to create new materials, but also to discover new possibilities with well-known polymer
58 properties like lower critical solution temperature autonomously modulated by photo-regulation [36]. Despite
59 the accomplishments already reached, the self-oscillating field still has a high potential, with recent progress
60 achieved to precisely control the mechanical oscillation[37,38], or simply by getting even closer to what nature
61 is capable of. Indeed, in all the biological phenomena, the cellular membrane is a wonderful model because of
62 the astonishing possibilities of action, from formation to self-destruction, only triggered by the membrane
63 environment. Being able to reach this complexity level would resolve most of the issues in the membrane field.
64 To achieve this objective, our group recently introduced the concept of self-oscillating filtration membranes
65 [39]. From an alumina membrane functionalized by a pH-sensitive polymer, pH oscillations in the filtration cell
66 made it possible to obtain transmembrane flux oscillations. The principle relies on a change in conformation of a
67 polymer chain as a function of the pH which leads to cycles of opening and closing of the membrane pores.

68 Here a new strategy is proposed to explore a universal method of introducing self-oscillation functionality to
69 all types of membranes, in particular polymer membranes. The overall strategy is depicted in Figure 1. The

70 principle is based on the synchronization between a pH oscillator, here Bromate-Sulfite-Ferrocyanide (BSF) and
 71 a membrane made pH-sensitive. To obtain this membrane, poly(methacrylic acid) (PMAA) was chosen as a pH-
 72 sensitive polymer thanks to its pKa at 4.8 [39]. PMAA is synthesized by Reversible Addition-Fragmentation
 73 Chain Transfer (RAFT) polymerization of tert-butyl methacrylate (tBuMA), followed by hydrolysis of the
 74 resulting PtBuMA. After aminolysis of the RAFT end group, the PMAA chains are terminated by a thiol
 75 function which will be used subsequently for their grafting onto the membrane. To make this grafting possible
 76 regardless of the type of membrane, a thin layer of polydopamine is first deposited. A Michael thiol-ene reaction
 77 between PMAA and polydopamine then allows membrane functionalisation. In the presence of the pH oscillator,
 78 cycles of change in the conformation of the PMAA chains allow for a cyclic change of the pore size and
 79 therefore of the transmembrane flux. In this work, the influence of the polydopamine deposition time and the
 80 PMAA molecular weight on the oscillation properties is particularly studied.



81

82 Figure 1 - General strategy carried out to produce self-oscillating polymer membranes

83 2. Experimental Part

84 2.1 Materials

85 Tert-butyl methacrylate 98%, containing 200 ppm monomethyl ether hydroquinone as inhibitor (Sigma) was
 86 filtered through an inhibitor removing resin for 15 minutes before use. Azobisisobutyronitrile (Fluka) was used
 87 after two recrystallizations in methanol. 4-cyano-4-(phenylcarbonothioylthio)pentanoic acid (Sigma), 1-
 88 Hexylamine (Fluka, 99%), chlorohydric acid 37% in weight, (trimethylsilyl)diazomethane solution 2.0 M in
 89 diethyl ether (Sigma) dopamine hydrochloride (Sigma), tris glycine buffer solution 10x concentrate (Sigma),
 90 potassium bromate (Sigma), bromocresol green, dye content 95% (Sigma), potassium hexacyanoferrate(II)
 91 trihydrate (Sigma), sodium sulfite (Sigma), sulfuric acid 99.9% (Sigma), bovine serum albumine (Sigma),
 92 dextran from Leuconostoc with Mn= 6000 g.mol⁻¹, Mn= 70000 g.mol⁻¹, Mn= 100000 g.mol⁻¹, Mn= 200000
 93 g.mol⁻¹, Mn= 500000 g.mol⁻¹, Mn= 2 000000 g.mol⁻¹ (Sigma), were used as received. Commercial
 94 polyethersulfone membranes with MWCO = 100 kDa, 63.5 mm diameter (Millipore®, PBHK06210) were
 95 washed 1 h by immersion in MilliQ water with water being changed three times before use.

96

97 2.2. Synthesis and Membrane Functionalisation

98

99 2.2.1. RAFT Synthesis of poly(tert butyl methacrylate)

100

101 Tert-butyl methacrylate (tBuMA) is placed in a flask with DMF at [tBuMA]= 0.5g.mL⁻¹, and the number of
102 moles of AIBN and CTA corresponding to the target molar mass. As an example, the target ratio for M_nPMAA of
103 20000 g.mol⁻¹ is $\frac{n_{CTA}}{n_{AIBN}} = 5$ and $\frac{n_{monomer}}{n_{CTA}} = 141$. The solution is then degassed with nitrogen in an ice bath for 30
104 minutes. The reaction was carried out for 24 h at 70 °C. The polymer is then precipitated twice in a cold
105 methanol/water mixture 4:1(v:v) and dried at room temperature under vacuum for 24h.

106

107 2.2.2 Aminolysis of poly(tert-butyl methacrylate)

108

109 The aminolysis procedure reported by Whittaker and al. [40] was adapted as follows: in a flask, PtBuMa is
110 dissolved at a concentration of 6.5 ml/g in THF and cooled in an ice bath. A large excess of hexylamine
111 ($\frac{n_{hexylamine}}{n_{polymer}} = 20$) is cooled in an ice bath. The two solutions are placed in two separate flasks, before being
112 degassed with nitrogen for 30 minutes in an ice bath. The hexylamine solution is added to the polymer solution
113 by syringe under nitrogen flow. The reaction was carried out at room temperature for 20 hours. The polymer is
114 precipitated in a methanol/water mixture 4:1 (v:v) and dried at room temperature under vacuum for 24h.

115

116 2.2.3 Deprotection of PtBuMA-SH

117

118 The protocol reported by Cazares-Cortes et al. [41] was adapted as follows: aminolyzed PtBuMa is
119 dissolved in dioxane at a concentration [PtBuMA-SH] = 83 mg.mL⁻¹. Under stirring, an excess of HCl ($\frac{n_{HCl}}{n_{polymer}} = 10$)
120 is added dropwise, before allowing the reaction to reflux for 16 hours at 85°C. Approximately one third of
121 the solvent was then evaporated on a rotary evaporator before precipitating the polymer in cooled diethyl ether.

122

123 2.2.4 Methylation of PMAA to poly(methyl methacrylate) (PMMA)

124

125 In order to check the molecular weight distribution of PMAA in organic medium and avoid its
126 aggregation in water during its analysis, PMAA was methylated into poly(methyl methacrylate) (PMMA)
127 before being characterized in Size Exclusion Chromatography in tetrahydrofuran. The protocol reported by
128 Lacik et al. [42] was used and adapted as follows: PMAA is dissolved in a 1:1 (v:v) mixture of THF / water at a
129 concentration of 5mg/mL and placed in a flask. Trimethylsilyldiazomethane is then added dropwise with stirring

130 until the yellow color is constant and no further off-gassing occurs. The flask is left to stir until the solution has
131 completely decolorized (7h). The solution was then placed in a beaker in the fume hood and left in the open air
132 until the solvent had evaporated completely.

133

134 2.2.5 PDA coating on commercial membranes

135

136 The protocol reported by Lee et al. [43] was adapted as follows: in a first step, three 24 mm diameter
137 membranes are cut from the 64 mm commercial membrane, before being washed for 1 hour in Milli-Q water. A
138 pH = 8.5 solution is prepared using a 10: 1 Milli-Q water/tris glycine buffer solution. Dopamine is added to
139 obtain a concentration of 0.1 mg.mL⁻¹. Membranes are then immersed 15 minutes directly to the dopamine
140 solution under stirring (70 rpm). Once the reaction is complete, the membrane is washed directly with milli-Q
141 water, then subjected to an ultrasound bath for 15 minutes, and stored in milli-Q water/ethanol 95:5 (v:v).

142 2.2.6 PMAA-SH grafting on PDA-coated membranes

143

144 A 10⁻⁵ mol solution of PMAA is prepared in milli-Q water at pH = 8.5. The PDA-coated membrane is
145 placed in the solution, and the reaction is carried out at 55°C for 2h. Once the reaction is complete, the
146 membrane is rinsed with milli-Q water, subjected to an ultrasound bath for 15 minutes, and then stored in milli-
147 Q water/ethanol 95 : 5 (v : v).

148

149 2.3 Polymer and membrane characterization

150

151 2.3.1 Polymer analysis

152

153 Proton Nuclear Magnetic Resonance (¹H NMR) spectroscopy. The ¹H NMR analysis was performed
154 with a Bruker Advance 400 MHz spectrometer. Samples were prepared in deuterated CDCl₃ for PtBuMA and
155 MeOD for PMAA.

156 Size exclusion chromatography (SEC). Molecular weight distributions were assessed by SEC (Viscotek
157 TDA 305, Malvern) using THF as eluent at a flow rate of 1.0 mL/min on a Polymer Laboratories PL-GPC 50
158 instrument using two PL mixed C 5.0 μm columns at 35 °C and a refractive index detector. Calibration was done
159 using Varian polystyrene narrow standards. Between 1 and 5 mg of polymer was dissolved in 1 ml of a solution
160 of THF with 0.3% toluene (flow marker). The solution was filtered with a 0.22 μm filter before being introduced
161 into the SEC.

162 Fourier Transform Infrared (FTIR) spectroscopy. FTIR analysis was performed with the FTIR 710
163 Nicolet instrument (Thermo Electron Corporation). The analyses are performed in ATR mode with 64 scans and
164 a resolution of 82 in transmission mode.

165 UV-Vis Spectroscopy. Polymer solutions before and after aminolysis were prepared at the same
166 concentration. The analysis was performed in a glass cuvette with the UvLine connect series 940 (SECOMAM)
167 from 200 to 800 nm in absorbance.

168

169 2.3.2 Membrane characterization

170

171 Water Contact angle (WCA). The WCA analysis was conducted with the ILMS GBX and Digidrop
172 GBX software. The membrane is dried in an oven, before being glued to a support prior the analysis. WCA was
173 measured with a drop volume of approximately 1.7 μ L. About 10 measurements are made before being averaged
174 for each trial, and three trials are performed.

175 Scanning Electron Microscopy (SEM). SEM analyses were conducted using a Hitachi S-4500 (Tokyo,
176 Japan) device operating at spatial resolution of 1.50 nm at 15 kV energy. The samples of 1cm x 0,5 cm were
177 dried and coated with an ultrathin layer of electrically conducting platinum deposited by high-vacuum
178 evaporation. Energy-dispersive X-ray spectroscopy analysis (EDX) was taken with Zeiss EVO HD15
179 microscope coupled with an Oxford X-MaxNSDD EDX detector. Surface porosity has been obtained from
180 binarized SEM images using Image J[®] software with $\phi = \frac{Area_{pores}}{Area_{total\ surface}} \times 100$.

181 Gravimetric analysis. Sample gain in weight after functionalization was estimated on samples dried for
182 1 h in a vacuum oven at 50°C, before being weighed with a Precisa XT 220 A balance.

183 Porosity measurement. Membranes were previously weighed after drying for 2h in a vacuum oven at
184 50°C, before being placed under ultrasound for 1 hour in a beaker of 1-butanol until no more bubbles escape
185 from it. The membranes were then weighed directly after removal from the beaker and blotting excess of 1-
186 butanol from the membrane surface. The equation for measuring the porosity (P) is as follows [44]:

$$187 \quad P(\%) = \frac{(W_2 - W_1)\rho_1}{\rho_1 W_2 + (\rho_2 - \rho_1)W_1}$$

188 with W_1 = initial mass, W_2 = mass after immersion in 1-butanol, ρ_1 = polyethersulfone density (1.37 g.mol⁻¹) and
189 ρ_2 = 1-butanol density (0.8 g.mol⁻¹)

190 Sieving curves. Dextran of different molecular weights were used to prepare aqueous solutions at a
191 concentration of 1000 ppm. 10 ml was then poured into a dead end stirred filtration cell at 1 bar. The first 2mL
192 of permeated water were discarded, and the next 4mL were taken as permeate solution. The last 4mL remaining
193 in the filtration cell constituted the retentate solution. Membranes were washed 10 minutes in water under
194 ultrasounds between each attempt. The solution signal was then analyzed by a Water 2414 refractive index
195 detector.

196 Liquid-liquid porometry. It was conducted with PRM-2000-LL-R porometer from G.E.P.S. France.
197 Prior to the measurement, same amount of MilliQ water and 1-butanol was “mixed” and let to separate by
198 decantation in order to saturate the two phases. The aqueous and organic phases were then stored separately.

199 Before the porometry experiment, the membrane was completely soaked into the aqueous phase before being
200 placed in a porometer cell. Increasing pressure from 0 to 6 bar was applied on the organic phase side of the
201 membrane to progressively replace the aqueous phase.

202 Zeta potential measurement. The surface charge (zeta potential) of the membrane was estimated using
203 SurPASS electrokinetic analyzer (Anton Paar, GmbH, Graz, Austria) based on the streaming potential method.
204 Washed membrane samples were mounted in an adjustable gap cell and soaked in 1 mM KCl. The cell height
205 was fixed at 100 mm. The electrolyte solution was circulated in the cell between two pieces of membrane. The
206 zeta potential was calculated using the Helmholtz–Smoluchowski equation from the measured streaming current
207 as a function of pH.

208 X-Ray photoelectron spectrometry (XPS). XPS was carried out with the ESCALAB 250 device from
209 ThermoElectron. The excitation source was the monochromatic source, Al K α line (1486.6 eV). The surface
210 analyzed has a diameter of 500 μ m. Photoelectron spectra were calibrated in binding energy with respect to the
211 energy of the C-C component of carbon C1s at 284.8 eV.

212 pH analysis. The HI 5221 (Hanna) instrument was calibrated with pH 4, 7 and 9 buffer solutions.
213 Measurements were then recorded every second.

214 Chemical resistance. Resistance of the membranes to the acidic and alkaline environments was
215 estimated by comparing the initial water flux of the grafted membrane at 1 bar of pressure drop with the flux
216 after an immersion of the membrane during 15 days at pH=3 for acidic condition, and pH=10 for alkaline
217 condition.

218 Tensile test. Mechanical properties of the membrane were measured with a 5kN ProLine ZwickRoell
219 universal testing machine and screw grips of 10kN. A 1x2cm sample membrane was cut and placed on the screw
220 grip while still wet from the conservation solution. The measurement started with 2cm between the two screw
221 grips.

222

223 2.3.3 Water permeation analysis and acquisition of oscillations

224

225 The 22 mm diameter membrane was placed into a homemade stainless steel 22 ml dead-end filtration
226 cell. A 1L Amicon tank filled with MilliQ water was connected to the cell with adjustable pressure. Permeated
227 water was measured using a balance connected to the S232 Data Logger software with a 0.599s time step
228 acquisition. A conditioning step was applied to all membranes by applying a pressure drop of 4 bar during 30
229 minutes before any permeability measurement.

230 For a water permeation under pH oscillations, aqueous feed solutions separated in two tanks entered
231 premixed at the same flow rate into the dead end filtration cell (Figure SI28) (Tank 1: [KBrO₃]₀ = 75 mM and
232 [sodium bromocresol green]₀ = 2.15 · 10⁻³ mM; Tank 2: [Na₂SO₃]₀ = 70 mM, [K₄Fe(CN)₆]₀ = 15 mM, [H₂SO₄]₀ =
233 7.5 mM). BSF pH oscillator was set up in the filtration cell under pressure and the relative pH evolution was
234 monitored by video acquisition of the solution color change thanks to a pH indicator (bromocresol) (Figure

235 SI28). The pH oscillator allows cyclic variations of the pH with wide and regular amplitude of oscillations
 236 between 3.5 and 6.5 under the membrane filtration conditions (Figure SI24). The targeted k_0 value, which
 237 corresponds to the inverse of the residence time in the filtration cell, was $1 \cdot 10^{-3} \text{ s}^{-1}$.

238 2.3.4 Modeling of Bromide-Sulfite-Ferrocyanide (pH and ionic strength)

239

240 Bromate-sulfite-ferrocyanide (BSF) pH oscillator has been modeled as described in our previous work
 241 [39]. The system of Ordinary Differential Equations (ODE) that described chemical reactions was numerically
 242 solved using finite element software: COMSOL Multiphysics® 5.4. A variable time step was used to improve
 243 the numerical resolution. The evolution of ionic strength (I) during pH oscillations was carried out by taking into
 244 account the following ionic species:

245 Cations: Na^+ , H^+ , K^+

246 Anions: OH^- , HSO_4^- , SO_4^{2-} , SO_3^{2-} , HSO_3^- , BrO_3^- , Br^- , $\text{HFe}(\text{CN})_6^{3-}$, $\text{Fe}(\text{CN})_6^{4-}$

247 Ionic strength was calculated over time by the following equations:

$$248 \quad I = \frac{1}{2} \left(\sum_i C_i z_i^2 \right)$$

249 C_i , being the molar concentration of ion i and z_i being the charge number of ion i

$$250 \quad I = \frac{1}{2} ([\text{SO}_3^{2-}] \cdot (-2)^2 + [\text{HSO}_3^-] \cdot (-1)^2 + [\text{HSO}_4^-] \cdot (-1)^2 + [\text{SO}_4^{2-}] \cdot (-2)^2 + [\text{BrO}_3^-] \cdot (-1)^2$$

$$251 \quad + [\text{Br}^-] \cdot (-1)^2 + [\text{HFe}(\text{CN})_6^{3-}] \cdot (-3)^2 + [\text{Fe}(\text{CN})_6^{3-}] \cdot (-3)^2 + [\text{OH}^-] \cdot (-3)^2$$

$$252 \quad + [\text{Fe}(\text{CN})_6^{4-}] \cdot (-3)^2 + [\text{H}^+] \cdot (1)^2 + [\text{Na}^+] \cdot (1)^2 + [\text{K}^+] \cdot (1)^2$$

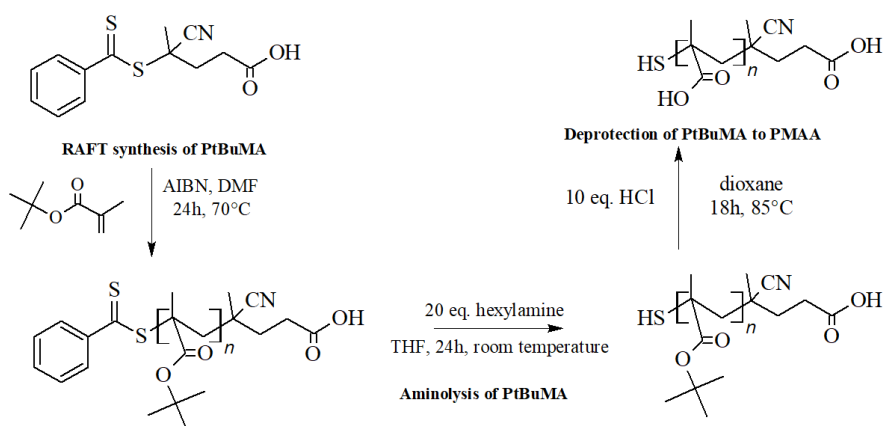
253

254

255 Results and Discussion

256

257 3.1 Polymer Synthesis



258

259 Scheme 1 – Overview of the thiol-functionalized polymethacrylic acid (PMAA) synthesis by RAFT
 260 polymerization

261 3.1.1 RAFT synthesis of PtBuMA

262

263 In a first step, a thiolated pH sensitive PMAA was prepared by RAFT polymerization of tBuMA
264 followed by its aminolysis and hydrolysis (Scheme 1). MAA was not polymerized directly as its corresponding
265 PMAA polymer is not soluble in an organic solvent and hard to characterize in water due to its inclination to
266 self-aggregate. The SEC curves of all PtBuMA polymers demonstrate distinct molecular weight distributions and
267 low dispersity as expected from a controlled polymerization (Figure SI-1). PtBuMA was obtained with monomer
268 conversions greater than 70% for all polymers (Table SI-1).

269 3.1.2 Aminolysis of PtBuMA

270

271 As previously explained, the grafting of PMAA onto the polymer membrane was carried out by a
272 Michael thiol-ene reaction on a deposited polydopamine top layer. For that, an aminolysis of the RAFT end
273 group is required to yield a thiol group at the end of the PtBuMa chain (Scheme 1).

274 The aminolysis was characterized by UV-visible spectroscopy following the absorbance peak at 300
275 nm, related to the aromatic RAFT end group. A large decrease in the signal attests to the success of the reaction
276 with a yield estimated up to 92% (Figure SI-2a, Table SI-1). The SEC curves before and after aminolysis (Figure
277 SI-2b) demonstrate the integrity of the polymer after the reaction, although some slight chain-chain coupling was
278 observed due to a thiol oxidation into disulphide.

279 3.1.3 Deprotection of PtBuMA from PMAA

280

281 The aminolyzed PtBuMA was then converted into PMAA by hydrolysis of the tert-butyl group. The
282 completion of the reaction is shown by the disappearance of the tert-butyl signal in ^1H NMR (Figure SI-6).

283 The FTIR spectra of the polymers were carried out after each step (Figure SI-3). The PtBuMA and
284 aminolyzed PtBuMA spectra are nearly identical as expected, since the very low concentration of the RAFT end
285 group does not enable any detection. Peak at 2992 cm^{-1} is assigned to the C-H stretching of alkane, and 1735 cm^{-1}
286 to the C=O stretching of ester group. After hydrolysis, FTIR spectrum of the resulting PMAA shows the
287 appearance of a peak at $3300\text{-}2500\text{ cm}^{-1}$ assigned to O-H stretching of the carboxylic acid group, as well as a
288 peak at 1715 cm^{-1} corresponding to the C=O stretching of the carboxylic acid group, in agreement with the ^1H
289 NMR.

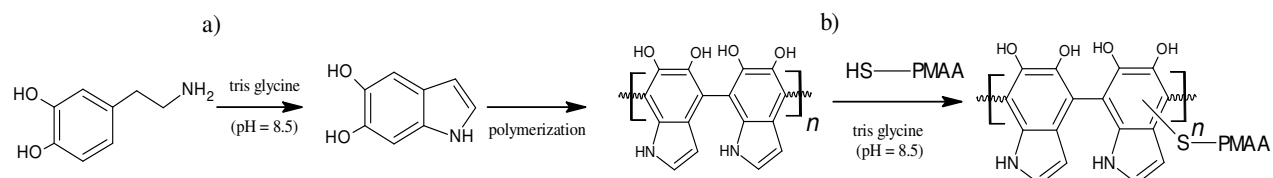
290 As previously reported [39], PMAA is difficult to characterize in aqueous SEC due to the presence of
291 aggregates. To check the distribution of molecular weights after hydrolysis of the tert-butyl group, PMAA was
292 methylated in poly(methyl methacrylate) (PMMA) and analyzed in THF SEC (Figure SI-4). A shift of the entire
293 distribution toward lower molecular weights is observed, as expected, with a maintained low dispersity of 1.06.
294 Note that the secondary pic corresponds to a double molecular weight, which is due to thiol-thiol coupling, as
295 explained before.

296

297

298 3.2 Membrane functionalisation

299



301

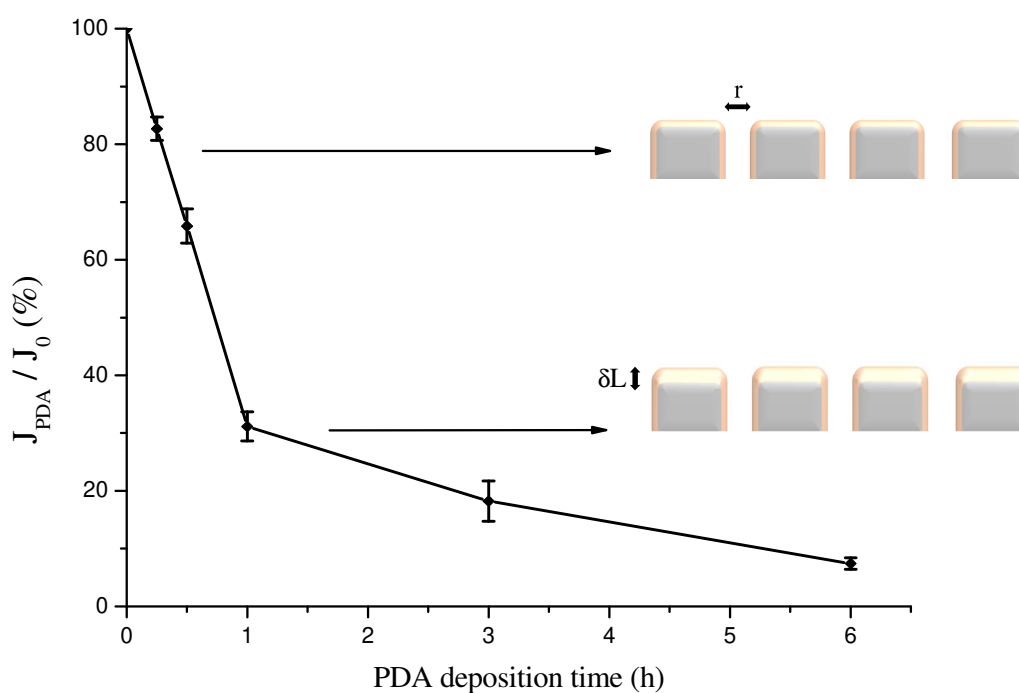


302

302 Figure 2 – a) Synthesis and coating of polydopamine onto polyethersulfone membrane followed by b) grafting of
303 pH-sensitive PMAA chains through Michael thiol-ene reaction.

304 The functionalisation of a commercial polyethersulfone membrane (PES) by the pH sensitive PMAA
305 was mediated through the deposition of a thin polydopamine (PDA) layer, as described in Figure 2. This
306 technique, already reported in the literature [45], is very versatile and can be applied to all types of membranes
307 without physicochemical constraints due to the ability of the PDA to stick anywhere. Polymer grafting was then
308 performed simply by immersion of the PDA-coated membrane in a PMAA solution. This functionalisation
309 process occurs in water under mild conditions, making any potential scale-up environmentally friendly.

310



311

312 Figure 3 – Evolution of the flux of the PES membrane after PDA deposition (J_{PDA}) compared to the flux of the
313 virgin membrane (J_0).

314

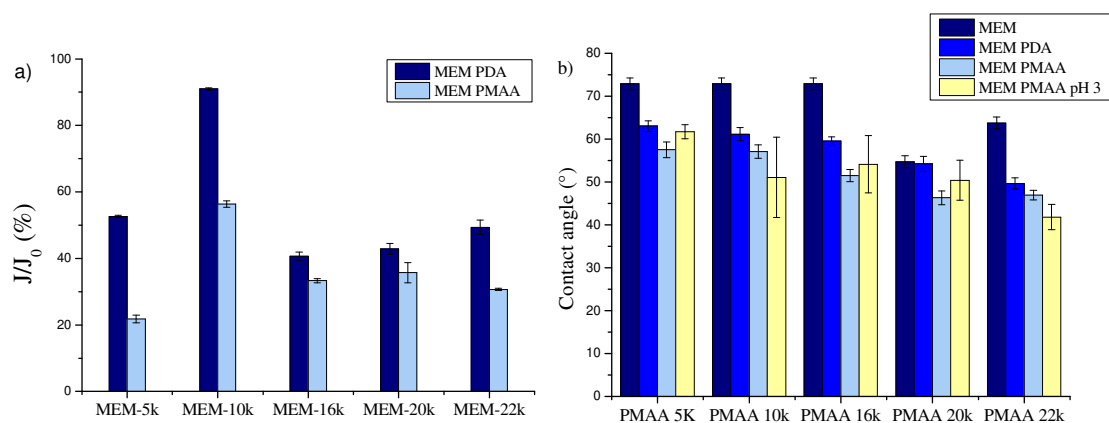
315 The permeance of the PDA coated membranes in Figure 3 shows a decrease correlated with the
316 deposition time. In a first part, delimited by a PDA deposition time of less than 1 hour, a significant slope is
317 observed while a clear break beyond this time marks a slower evolution. This distinction can illustrate two
318 different flux reduction mechanisms. As the Poiseuille equation (1) shows, the flux can evolve by a change in the
319 radius of the pores (to the power of 4), their number, and their length. Given the rapid evolution for short
320 deposition times, we can hypothesize that a decrease in the pore diameter is the main factor involved in this first
321 part. Then, the PDA coating increasing with time, the length of the pores, and the number of open pores certainly
322 govern the evolution of the flux in the second part.

323
$$J = \frac{N \cdot dP \cdot r^4}{8 \cdot \eta \cdot L} \quad (1)$$

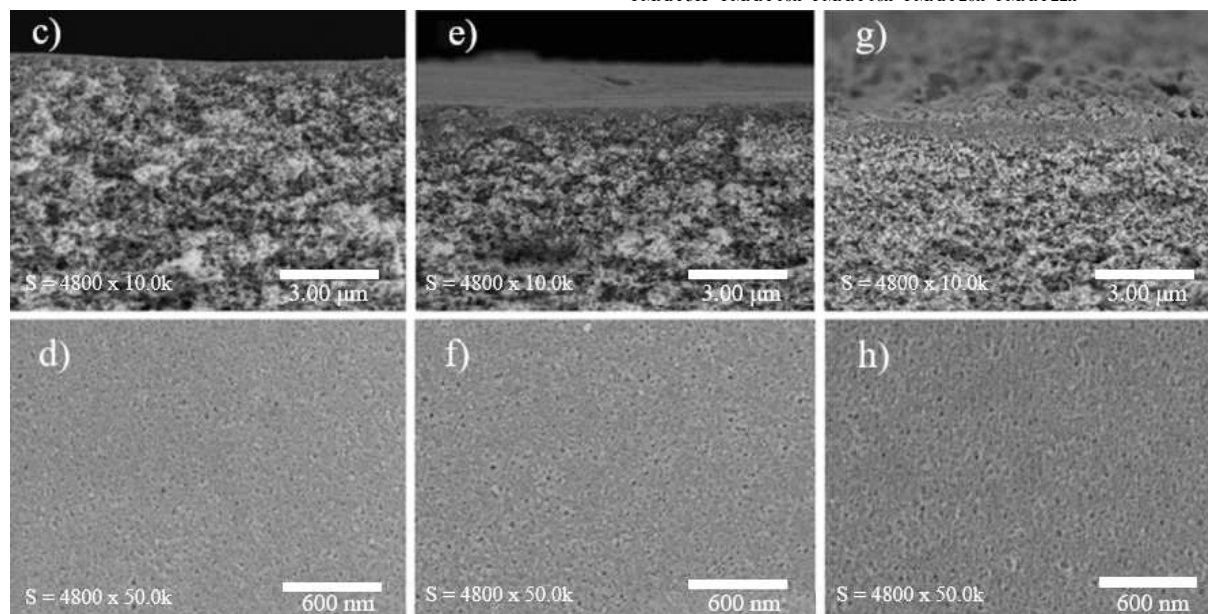
324 with J = transmembrane flux; N = pores number; dP = pressure gradient across the membrane; r = average pore
325 radius; L = membrane thickness; η = fluid viscosity.

326 A 15 min deposition time was selected for the rest of the work, which is a good compromise between enough
327 PDA functionalisation for the subsequent PMAA grafting and moderate flux decrease.

328



329



330

330 Figure 4 –a) Evolution of the flux (J) after PDA deposition and after PMAA grafting as normalized by the flux
 331 of the virgin membrane (J_0), as a function of PMAA molecular weight, b) Water contact angle on virgin PES
 332 membrane (MEM), PDA modified membrane (MEM PDA) and PMAA grafted membrane (MEM PMAA), c-h)
 333 SEM images of cross sections (c, e, g) and top surfaces (d, f, h) of virgin PES membrane (c, d), 15 min PDA
 334 coated PES membrane (e, f), and PMAA_{22k} grafted membrane (g, h).

335

336 The functionalisation was indirectly characterized by the flux measurement (Figure 4a). A flux decrease
 337 is observed after each functionalisation step from virgin PES membrane to PDA-modified membrane to PMAA-
 338 grafted membrane. However, the decrease does not appear to be correlated with the molecular weight of the
 339 grafted PMAA and ranges from 10 to 60% for the same PDA deposition time (15 min).

340 An increase of the surface hydrophilicity was also observed after each step, illustrated by the decrease
 341 of the water contact angle (Figure 4b). If the trend is clear and constant, the water contact angle seems to be
 342 sample dependent, with a dependence more relying on the varying surface roughness rather than the results of
 343 the PMAA molecular weight for instance. Switching the water pH of the droplets from 7 to 3 did not provide a
 344 clear tendency. It is assumed that it is the result of two antagonist effect: an acidic pH below the PMAA pKa will

345 result in the pore opening due to the polymer contraction. However, PMAA also became less hydrophilic at this
346 pH, as did the membrane surface.

347 Each step of membrane modification has been characterized by SEM (Figure 4c-h). Although the top
348 surface images do not show any real difference after functionalization steps, a thin layer of PDA and PMAA is
349 well observed in the cross-section images. The EDX mapping (Figure SI-8) shows that PMAA is uniformly
350 grafted with visible enrichment of carbon on the surface. The membrane bulk porosity was estimated from 1-
351 butanol gravimetric analysis and a stable value around 77% is found for all membranes (porosity_{MEM} = 77.5%;
352 porosity_{MEM PDA 15 min} = 77.7%; porosity_{MEM PMAA_10k} = 77.2%). Since only a surface modification is performed
353 on an asymmetric PES membrane, the overall porosity is in return not affected. On the contrary, the time of PDA
354 deposition is found to change surface porosity, as measured by SEM image treatment (porosity_{MEM} = 7.8%;
355 porosity_{MEM PDA 15 min} = 3.4%; porosity_{MEM PDA 1 h} = 3.5%; porosity_{MEM PDA 18 h} = 1.5%). Similar trend is
356 observed with PMAA grafting, which reduces surface porosity (porosity_{MEM PMAA_22k (with PDA=15 min)} = 2.3%), in
357 agreement with a polymer coating/grafting.

358 Gravimetric analysis was carried out to estimate the weight of polymer deposited at the membrane
359 surface after PDA coating and PMAA grafting (Table SI-3). As expected, a correlation between the PDA
360 deposition time and the PDA quantity deposited is observed. Because PMAA is grafted onto the PDA layer, a
361 direct link is observed between the quantity of PDA deposited and the yield of PMAA grafting. Interestingly, for
362 the same PMAA grafting time, the grafted PMAA was 2.4 times higher when the deposited PDA was higher.
363 Here it is suspected that 18h PDA coating has increased surface roughness and thus the specific PDA surface
364 available for PMAA grafting. Young moduli (tensile test) were measured to see if the PMAA grafting would
365 have an impact, but it appears that the deposition is too thin to make any significant difference (Table SI-4).

366 The surface composition was characterized by XPS analysis (Figure SI-9-19). However, unless a
367 sufficient PDA layer is deposited (18h), the elemental compositions (C, N, O and S) of the PDA coated
368 membranes remain similar to the PES commercial membrane. This is a further proof that the PDA deposition
369 time chosen (15 minutes) allows a very thin layer to be deposited, sufficient to be able to functionalize without
370 drastically changing the chemical nature of the interface. The XPS data (Table SI-5) shows that the carbon and
371 nitrogen concentrations in PMAA grafted membranes are similar than in the commercial membrane, but the
372 oxygen concentration rises with the polymer grafting, which is in line with the theory. It also appears that the
373 sulfur concentration decreases for all the grafted samples, proving that deposition on the PES membrane is
374 taking place.

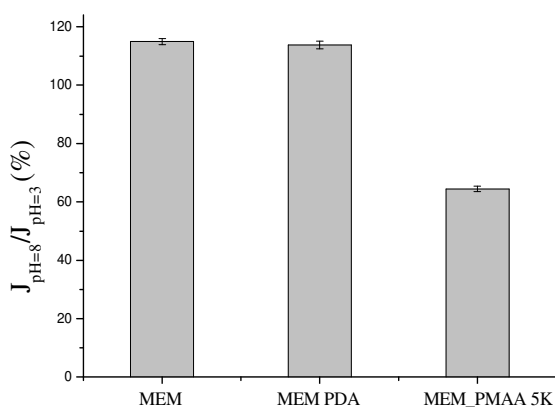
375 A measurement of the streaming potential was performed (Figure SI-7). A significantly different
376 evolution of the calculated negative zeta potential is observed, attesting to the difference in surface chemistry.
377 However, a similar isoelectric point (IEP) at pH 3-3.5 for the three samples, in agreement with reported PES
378 IEP[46], suggests that only a partial coverage of the membrane surface occurs.

379

380 3.3 pH-induced self-oscillating flux

381

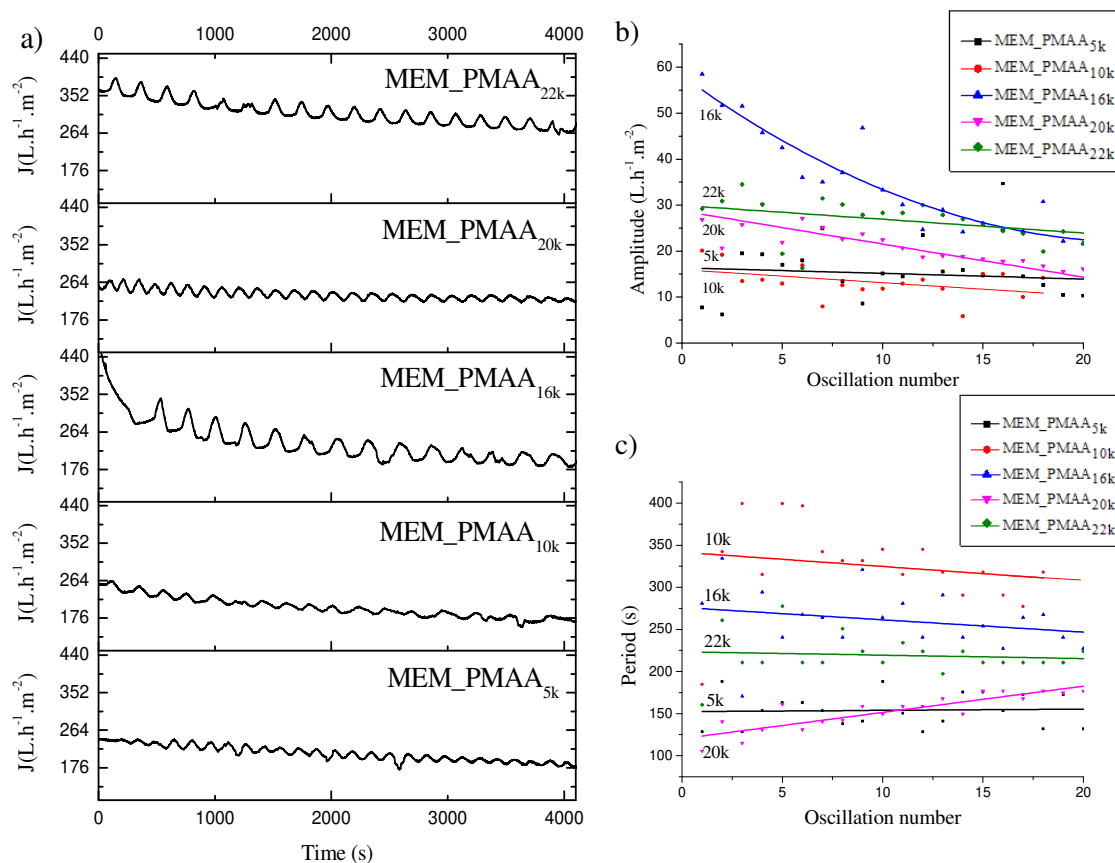
382 In order to yield a self-oscillating behavior, a pH-sensitive polymer membrane is mounted into a dead-
 383 end filtration cell and synchronized with a pH oscillator (Figure SI-26). PMAA is a weak polyelectrolyte with a
 384 quick conformation change as a function of pH. A globular conformation is observed for low degrees of
 385 ionization, and the chains are collapsed due to the "hydrophobic" interactions with the methyl groups. The
 386 membrane pores are then in an "open" state. The polymer chains expand abruptly above a pH threshold ($pK_a =$
 387 4.8) to release the electrostatic energy associated with deprotonation. The membrane pores are "closed" at this
 388 point. The BSF pH oscillator can generate pH cycles ranging from 3.5 to 6.5 (Figure SI-22). The BSF oscillator
 389 and the pH-sensitive membrane must be synchronized in order for the membrane pores to vary cyclically and to
 390 thus observe a periodic variation of the transmembrane flux. The first step is to check the "unresponsiveness" of
 391 the virgin PES membrane to pH in terms of water permeability. Thus, the virgin PES membrane was subjected to
 392 sequential pH variations (3 and 7) (Figure SI-20). Ignoring the effect of the depressurization of the filtration cell
 393 during the change of solutions, no significant change in flux was observed in relation to the pH. One can note a
 394 natural tendency of transmembrane flux decrease over time despite the conditioning performed (see experimental
 395 part for more details).



396
 397 Figure 5 – Water flux ratio at pH 8 and 3 of the commercial PES membrane (MEM), the membrane coated with
 398 PDA for 15 min (MEM_PDA), and the membrane grafted with PMAA_{5k} (MEM_PMAA_{5k}) at $\Delta P = 1$ bar.

399 The pure water flux of the virgin PES membrane, the PDA coated membrane, and the PMAA grafted
 400 membrane were then measured at pH values above and below the PMAA pK_a to assess its effect (Figure 5).
 401 Whereas a slight increase in flux at basic pH is observed for commercial and PDA covered membranes, a clear
 402 flux decreases of 40% at pH=8 is measured when PMAA is grafted onto the membrane. Indeed, above PMAA
 403 pK_a value, the polymer is in an expanded conformation which obstructs the pores and reduces their size. Since
 404 the dependence is inversed compared to the PDA coated membrane, it can be deduced that PMAA membrane is
 405 pH-sensitive and that a modulation of the pH results in a proportionate change in the water permeability. It
 406 should be noted that the tolerance of the membrane towards acidic and alkaline operating conditions was
 407 checked to avoid any misinterpretation. The water flux at $\Delta P = 1$ bar of the virgin PES membrane and the
 408 PMAA grafted membrane was measured at pH 3 and 10 for 15 days without showing any significant change
 409 ($J_{PES\ MEM, pH3} = 278 \pm 51$ L.h⁻¹.m⁻²; $J_{PES\ MEM, pH10} = 181 \pm 24$ L.h⁻¹.m⁻²; $J_{PMAA\ MEM, pH3} = 125 \pm 3$ L.h⁻¹.m⁻²; $J_{PMAA\ MEM, pH10} = 129 \pm 5$ L.h⁻¹.m⁻²).

411 As explained before, autonomous cyclic pH change will be carried out thanks to the BSF chemical
 412 oscillator setup in the filtration cell. BSF is an oscillating network of chemical reactions, which can be
 413 summarized by a set of 7 reactions [39] (Table SI-6). The cyclic predominance of certain reactions in the BSF
 414 oscillator leads to a modulation of the pH within a domain of residence time in the filtration cell. The residence
 415 time domain to observe the pH oscillations was previously estimated from the construction of a bifurcation
 416 diagram (Figure SI-21) [39] and a k_0 value of 10^{-3} s^{-1} was targeted in this work, k_0 being the inverse of the
 417 residence time in the filtration cell. The pH oscillations produced from a BSF oscillator for a k_0 of 10^{-3} s^{-1} have
 418 an average period of about 390 s after stabilization with a pH varying cyclically and continuously between 3 and
 419 6.5 (Figure SI-22). PMAA pKa being around 4.8, then the pH oscillations will enable change of conformation of
 420 PMAA chains grafted on the membranes. Because of the inability to directly follow the pH change in a
 421 pressurized filtration cell, a colored indicator was used to visually track the pH oscillation. The BSF reaction
 422 alone was filmed and monitored by a pH-meter to see if the colored indicator is a reliable tracking system



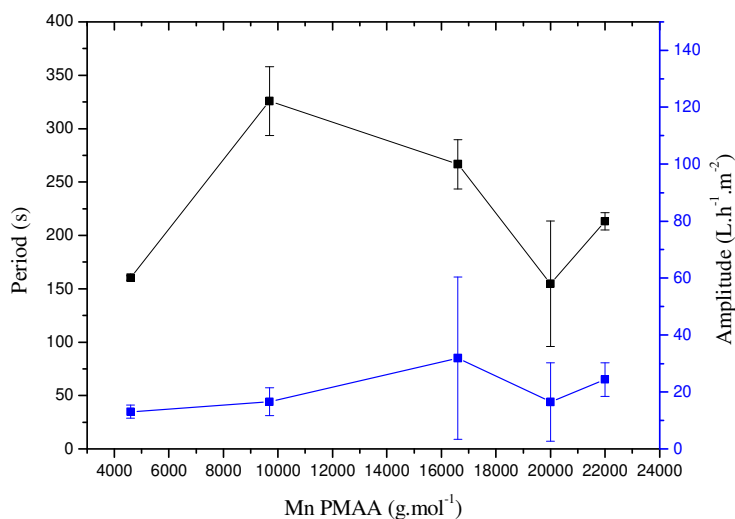
423 (Figure SI-23). It appears that the visual color change and the pH change match perfectly.

424

425 Figure 6 – a) Self-oscillating flux of functionalized membranes synchronized with a BSF oscillator with the
 426 following conditions: $[\text{KBrO}_3]_0 = 75 \text{ mM}$, $[\text{Na}_2\text{SO}_3]_0 = 70 \text{ mM}$, $[\text{K}_4\text{Fe}(\text{CN})_6]_0 = 15 \text{ mM}$, $[\text{H}_2\text{SO}_4] = 7.5 \text{ mM}$ for T

427 = 30 °C and $k_0 = 10^{-3} \text{ s}^{-1}$; b) Evolution of oscillation amplitude for each PMAA molecular weight; c) Evolution
428 of oscillation period for each PMAA molecular weight. b-c) Fitting curves are shown only as a guide for the eye

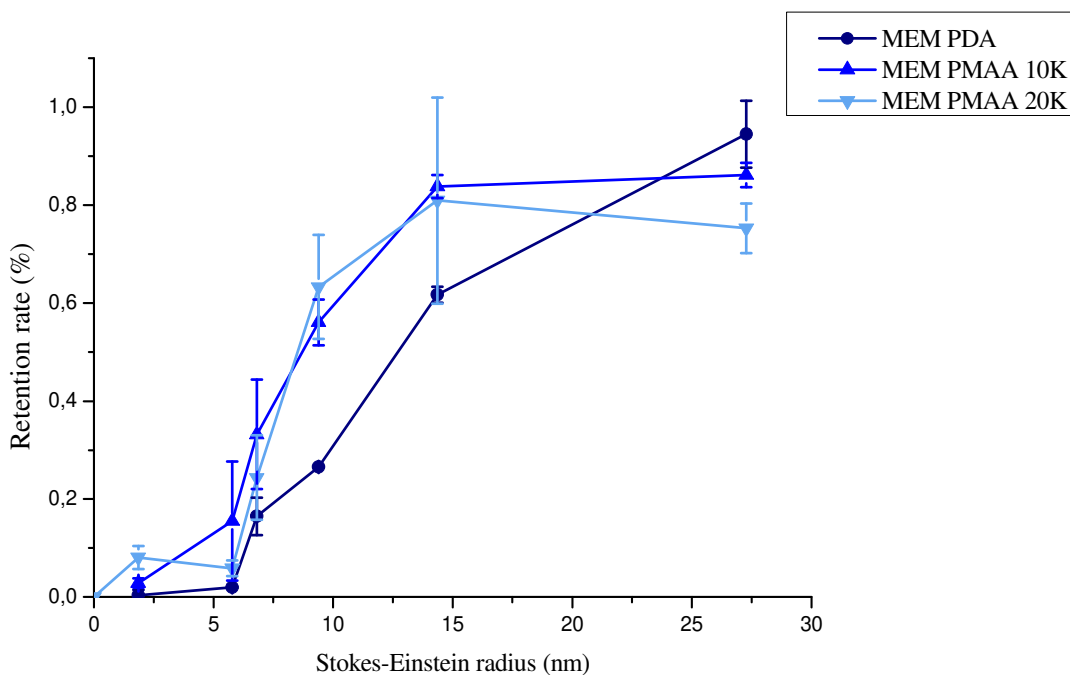
429 When the BSF pH oscillator is set up in the filtration cell with PMAA-functionalised PES membranes,
430 flux oscillations are observed as shown in Figure 6a. It appears that the molecular weight of PMAA greatly
431 affects the flux oscillations, as much in amplitude than in period. Also, the BSF oscillator seems to be able to
432 have a great stability under filtration conditions as self-oscillating flux could still be recorded after 35 cycles of
433 pH (Figure SI-27). Figure 6b shows that there is a more or less pronounced decrease of the oscillation amplitude
434 in time, with a variable intensity depending on the PMAA molecular weights. The PMAA chains remain
435 hydrophilic all the time including below the pKa of the PMAA. However, as reported in literature, the grafted
436 polymer onto the membrane surface may not be fully accessible to the bulk solution and some charges can
437 remain avoiding a complete polymer collapsing over the cycles [47]. It can be noted that the greatest decrease in
438 amplitude was observed with MEM_PMAA16k. The oscillation periods represented in Figure 6c remain
439 relatively stable over time, except for MEM_PMAA20k, for which a slight increase is observed over time. As
440 the oscillation period depends on the oscillator mechanism, it is complex to analyse the evolutions. However, it
441 appears that all the periods are shorter than for the BSF oscillator alone, which shows that the membrane
442 participates in the oscillating system. The molecular weight of the grafted PMAA appears to modulate both the
443 period and the amplitude, as summarized in Figure 7.



444
445 Figure 7 - Average amplitude and period of water flux oscillations for each PMAA molecular weight

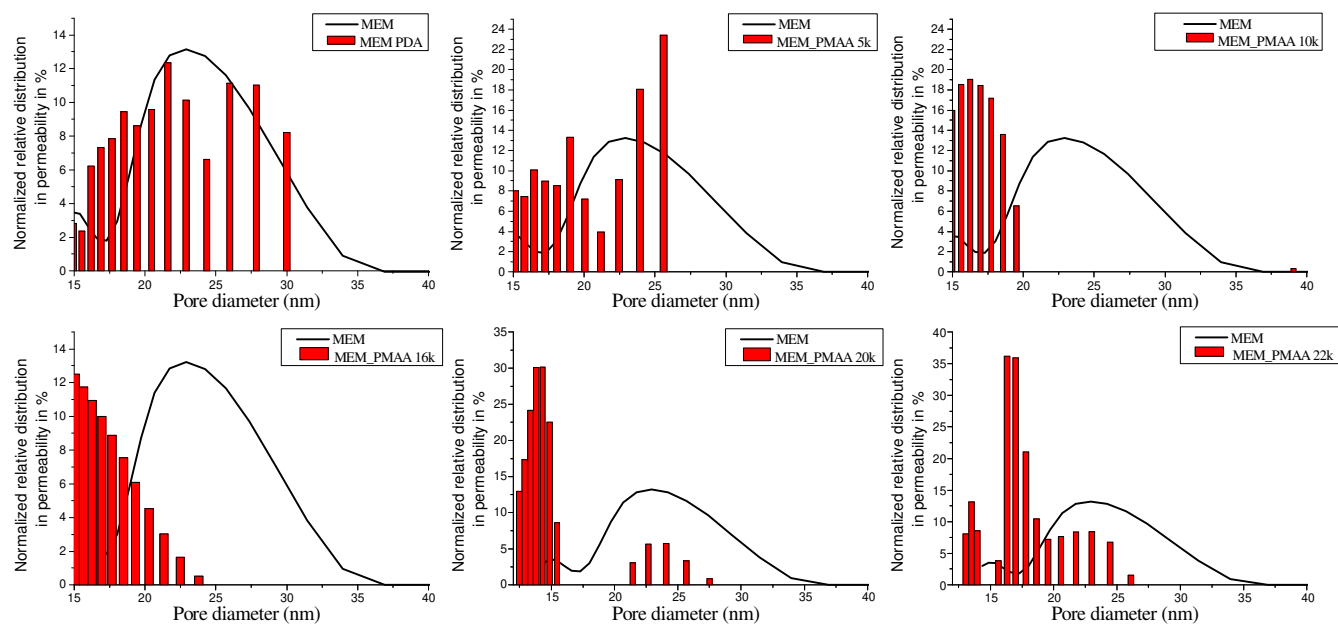
446 When the two parameters are compared in Figure 7, it appears that both values increase with the
447 molecular weight of PMAA, then decrease for PMAA_{20k}, before increasing again at PMAA_{22k}. A hypothesis is
448 that a steric exclusion occurs between Mn= 16 000 g.mol⁻¹ and 20 000 g.mol⁻¹. A large amplitude can be
449 observed when the PMAA is located inside the pores. When the PMAA chain length is increased, the flux
450 change, corresponding to the compact and extended conformations of PMAA in the pores, is larger. However,
451 above a threshold value of PMAA molecular weight, some steric hindrance can occur, preventing grafting inside
452 the pores and thus leading to a decrease in the flux oscillation amplitude. A second increase above 20 000 g.mol⁻¹
453 is also observed which can be explain by an obstruction of the pores from the membrane surface. If the

454 hypothesis is correct, the pore size distribution for MEM_PMAA_{10k} and MEM_PMAA_{20k} would be significantly
455 different. Indeed, MEM_PMAA_{10k} would have a reduced pore size due to the presence of the polymer chains in
456 the pores, whereas grafting of MEM_PMAA_{20k} would have a lower pore size impact, being mostly located at the
457 membrane surface. The sieving curves, carried out with dextran of different molecular weights, are presented in
458 Figure 8.



459
460 Figure 8 – Sieving curve for ●) PDA coated membrane ▲) grafted membrane with PMAA =10 000 g.mol⁻¹ and
461 ▼) grafted membrane with PMAA =20 000 g.mol⁻¹

462
463 The sieving curves were measured for two grafted PMAA molecular weights, PMAA_{10k} and PMAA_{20k}.
464 It should be first mentioned that a weak reproducibility was observed when repeating the sieving curve
465 measurements on different samples of the same membrane as illustrated by the large error bars obtained for the
466 virgin PES membrane (Figure SI-28) [48]. To try to overcome its impact, the sieving curves were made on the
467 same membrane for all the functionalisation steps (Figures 8). It appears that the PDA deposition has not clearly
468 shifted the sieving curve towards lower pore values as expected, which could be explained by a change in the
469 surface properties (hydrophilicity, roughness) counterbalancing the pore size decrease. Grafting of PMAA has
470 shifted the sieving curve to lower pore size, in agreement with the flux decrease observed previously. However,
471 considering the error bars, the sieving curves as measured with the two PMAA molecular weights did not
472 highlight a significant difference.



473

474 Figure 9 – Liquid-liquid porometry results for PES commercial membrane, PDA-coated membrane (15 min) and
 475 membranes grafted with PMAA of different molecular weights.

476 Liquid-liquid porometry (Figure 9) shows that the commercial membrane has an average pore size of 22 nm and
 477 a relatively large dispersity. The PDA deposition doesn't seem to affect significantly the pore size distribution.
 478 However, when PMAA is grafted, the pore size distribution is shifted towards lower values in all cases, showing
 479 that PMAA grafting is decreasing the pore size with a higher shift towards lower pore size with increasing
 480 PMAA molecular weight, in agreement with the evolution of the water flux as previously discussed. However,
 481 for the membranes grafted with PMAA $\geq 20\ 000\ \text{g}\cdot\text{mol}^{-1}$, a double distribution is observed with smaller pores as
 482 in the case observed with PMAA lower than $20\ \text{kg}\cdot\text{mol}^{-1}$, but also with a remaining distribution of pore size from
 483 the initial PDA membrane. A hypothesis is that a partial steric exclusion of PMAA from the membrane pores
 484 appended leading to leave unfunctionalized a part of the initial pore size distribution. This is in agreement with
 485 the break in water flux amplitude trend observed in Figure 7 at this PMAA molecular weight. We didn't succeed
 486 in showing a clear shift of the pore size distribution from the sieving curves or from the porometry measurement
 487 when comparing the results at pH below and above the PMAA pKa (data not shown). To understand that
 488 observation, the expected pore size variation resulting from a pH below and above the PMAA pKa was
 489 estimated from the measured water flux variations according to the Poiseuille law (equation 1) (Table SI-7).

490 A pore size change of maximum 2.5 to 6.5% (0.4 to 1.5 nm) is expected which explains the difficulty to directly
 491 observe it following the pore size. It is however clearly visible in the flux measurement thanks to dependence of
 492 the flux to the fourth power of the pore radius. We can therefore conclude that water flux self-oscillations have
 493 been yielded without significantly alter the solute retention of membrane.

494 The BSF oscillator involves many ionic species whose concentration can vary with time depending on the
 495 oscillatory regime. Given our use of a weak polyelectrolyte (PMAA), the impact of ionic strength on water
 496 permeation results was checked. For this, the ionic strength of the oscillator ($400\ \text{mmol}\cdot\text{L}^{-1}$) was reproduced by
 497 adding NaCl ($0.4\ \text{mol}\cdot\text{L}^{-1}$) to water. As shown in Figure SI-25, the transition from pure water to salted water was

498 not accompanied by a change in flux. In addition, a theoretical modeling of pH and ionic strength oscillations
499 was performed (Figure SI-24) and only a weak ionic strength oscillation is observed between 414 and 420
500 mmol.L⁻¹. Thus, we can conclude that the ionic strength imposed by the pH oscillator does not impact the water
501 permeation results. The flux oscillations are therefore only the results of the expansion-contraction cycles of the
502 PMAA inside the membranes pores.

503 3. Conclusions

504

505 Self-oscillating polymer membranes showing continuous periodic flux evolution have been successfully
506 prepared. The flux oscillations were obtained by coupling a pH-sensitive polymer membrane to a pH oscillator
507 (BSF). For this, PMAA was synthesized with different molecular weights and grafted onto a commercial PES
508 membrane via an intermediate layer of PDA. Each stage of polymer manufacturing and membrane
509 functionalisation has been precisely characterized. Secondly, the pH oscillator was stabilized in a filtration cell
510 and brought into contact with the pH-sensitive membrane. The PMAA grafted onto the membrane responds
511 almost instantaneously to changes in pH and oscillates between two chain conformations (extended and
512 collapsed). Therefore, an autonomous and cyclic membrane pore size change was observed leading to the self-
513 oscillation of the membrane water flux. Interestingly, although water flux is periodically modulated, the
514 corresponding pore size change due to the pH modulation is estimated to be less than 6%, which has
515 immeasurable impact on the solute retention of membrane. In addition, the amplitude of the flux cycles can be
516 modulated by the molecular weight of the PMAA grafted onto the membrane until a threshold value of 20 000
517 g.mol⁻¹, above which a polymer exclusion from the pores was observed. In perspective to this work, the effect of
518 flux oscillations on the challenging fouling phenomenon will be explored since a perpetual change of the
519 membrane surface properties combined with an adhesion of retained species hampered by flux oscillations could
520 offer a more sustainable alternative to the usual mechanical and chemical membrane cleanings. Bringing self-
521 oscillating behaviour to a polymer filtration membrane represents a further step towards the design of
522 autonomous membranes.

523

524 Credit authorship contribution statement

525 **Johanne Pirkin-Benameur**: Conceptualization, Methodology, Data curation, Writing – original draft, Writing –
526 review & editing. **Denis Bouyer**: Conceptualization, Methodology, Data curation. **Damien Quemener**:
527 Conceptualization, supervision, acquisition of funds, data curation, writing - review & editing.

528

529 Declaration of Competing Interest

530 The authors declare no conflict of interest.

531 Acknowledgements

532 The authors thank the Institut Universitaire de France (IUF) and the Agence Nationale de la Recherche (ANR)
533 through the OscMEM project (ANR-20-CE06-0013-01) for financial support. Valérie Flaud, Didier Cot, and
534 Bertrand Rebiere are acknowledged for XPS, SEM, and EDX analysis.

535 References

536

- 537 [1] L. Persson, B.M.C. Almroth, C.D. Collins, S. Cornell, C.A. de Wit, M.L. Diamond, P. Fantke, M.
538 Hassellöv, M. MacLeod, M.W. Ryberg, P.S. Jørgensen, P. Villarrubia-Gómez, Z. Wang, M.Z.
539 Hauschild, Outside the Safe Operating Space of the Planetary Boundary for Novel Entities,
540 Environmental Science & Technology. (2022) acs.est.1c04158.
541 <https://doi.org/10.1021/ACS.EST.1C04158>.
- 542 [2] M. Wei, Y. Gao, X. Li, M.J. Serpe, Stimuli-responsive polymers and their applications, Polymer
543 Chemistry. 8 (2016) 127–143. <https://doi.org/10.1039/C6PY01585A>.
- 544 [3] D. Roy, W.L. A. Brooks, B. S. Sumerlin, W.L.A. Brooks, B.S. Sumerlin, New directions in
545 thermoresponsive polymers, Chemical Society Reviews. 42 (2013) 7214–7243.
546 <https://doi.org/10.1039/C3CS35499G>.
- 547 [4] S. Dai, P. Ravi, K. Chiu Tam, K.C. Tam, {pH}-Responsive polymers : synthesis, properties and
548 applications, Soft Matter. 4 (2008) 435–449. <https://doi.org/10.1039/B714741D>.
- 549 [5] D.A. Davis, A. Hamilton, J. Yang, L.D. Cremer, D. Van Gough, S.L. Potisek, M.T. Ong, P. V.
550 Braun, T.J. Martínez, S.R. White, J.S. Moore, N.R. Sottos, Force-induced activation of covalent
551 bonds in mechanoresponsive polymeric materials, Nature 2009 459:7243. 459 (2009) 68–72.
552 <https://doi.org/10.1038/nature07970>.
- 553 [6] Y.L. Colson, M.W. Grinstaff, Y.L. Colson, M.W. Grinstaff, Biologically Responsive Polymeric
554 Nanoparticles for Drug Delivery, Advanced Materials. 24 (2012) 3878–3886.
555 <https://doi.org/10.1002/ADMA.201200420>.
- 556 [7] A. Fernández-Nieves, Engineering colloids with optical and geometrical anisotropies: de-
557 coupling size monodispersity and particle properties, Soft Matter. 2 (2006) 105–108.
558 <https://doi.org/10.1039/B512441G>.
- 559 [8] N.S. Terefe, O. Glagovskaia, K. De Silva, R. Stockmann, Application of stimuli responsive
560 polymers for sustainable ion exchange chromatography, Food and Bioproducts Processing. 92
561 (2014) 208–225. <https://doi.org/10.1016/J.FBP.2014.02.003>.
- 562 [9] G.W. De Groot, M.G. Santonicola, K. Sugihara, T. Zambelli, E. Reimhult, J. Vörös, G.J. Vancso,
563 Switching transport through nanopores with pH-responsive polymer brushes for controlled
564 ion permeability, ACS Applied Materials and Interfaces. 5 (2013) 1400–1407.
565 https://doi.org/10.1021/AM302820Y/SUPPL_FILE/AM302820Y_SI_001.PDF.
- 566 [10] X. Gao, W. Yang, P. Pang, S. Liao, Q. Cai, K. Zeng, C.A. Grimes, A wireless magnetoelastic
567 biosensor for rapid detection of glucose concentrations in urine samples, Sensors and
568 Actuators B: Chemical. 128 (2007) 161–167. <https://doi.org/10.1016/J.SNB.2007.05.045>.
- 569 [11] D. Schmaljohann, Thermo- and pH-responsive polymers in drug delivery, Adv Drug Deliv Rev.
570 58 (2006) 1655–1670. <https://doi.org/10.1016/J.ADDR.2006.09.020>.

- 571 [12] X. Yang, L. Chen, B. Huang, F. Bai, X. Yang, Synthesis of pH-sensitive hollow polymer
572 microspheres and their application as drug carriers, *Polymer (Guildf)*. 50 (2009) 3556–3563.
573 <https://doi.org/10.1016/J.POLYMER.2009.06.027>.
- 574 [13] P. Zarrintaj, M. Jouyandeh, M.R. Ganjali, B.S. Hadavand, M. Mozafari, S.S. Sheiko, M.
575 Vatankhah-Varnoosfaderani, T.J. Gutiérrez, M.R. Saeb, Thermo-sensitive polymers in
576 medicine: A review, *European Polymer Journal*. 117 (2019) 402–423.
577 <https://doi.org/10.1016/J.EURPOLYMJ.2019.05.024>.
- 578 [14] J.B. Qu, L.Y. Chu, M. Yang, R. Xie, L. Hu, W.M. Chen, A pH-Responsive Gating Membrane
579 System with Pumping Effects for Improved Controlled Release, *Advanced Functional*
580 *Materials*. 16 (2006) 1865–1872. <https://doi.org/10.1002/ADFM.200500897>.
- 581 [15] G. Yi, X. Fan, X. Quan, H. Zhang, S. Chen, H. Yu, A pH-responsive PAA-grafted-CNT intercalated
582 RGO membrane with steady separation efficiency for charged contaminants over a wide pH
583 range, *Separation and Purification Technology*. 215 (2019) 422–429.
584 <https://doi.org/10.1016/J.SEPPUR.2019.01.028>.
- 585 [16] Z. Chen, M.H.-Y. Chan, V.W.-W. Yam, Stimuli-Responsive Two-Dimensional Supramolecular
586 Polymers Based on Trinuclear Platinum(II) Scaffolds: Reversible Modulation of
587 Photoluminescence, Cavity Size, and Water Permeability., *J Am Chem Soc.* (2020).
588 <https://doi.org/10.1021/jacs.0c07969>.
- 589 [17] Q. Ye, R. Wang, C. Chen, B. Chen, X. Zhu, High-Flux pH-Responsive Ultrafiltration Membrane
590 for Efficient Nanoparticle Fractionation., *ACS Applied Materials & Interfaces*. (2021).
591 <https://doi.org/10.1021/acsami.1c16673>.
- 592 [18] Z. Ma, G. Shu, X. Lu, Preparation of an antifouling and easy cleaning membrane based on
593 amphiphobic fluorine island structure and chemical cleaning responsiveness, *Journal of*
594 *Membrane Science*. (2020). <https://doi.org/10.1016/j.memsci.2020.118403>.
- 595 [19] J. Qiao, L. Liu, J. Shen, L. Qi, Enzyme immobilization on a pH-responsive porous polymer
596 membrane for enzymatic kinetics study, *Chinese Chemical Letters*. 32 (2021) 3195–3198.
597 <https://doi.org/10.1016/J.CCLET.2021.03.021>.
- 598 [20] K. Aissou, H. Bouzit, F. Krusch, J.P. Méricq, D. Cot, N. Masquelez, S. Roualdes, D. Quémener,
599 Asymmetric Solvent-Annealed Triblock Terpolymer Thick Films Topped by a Hexagonal
600 Perforated Lamellar Nanostructure, *Macromol Rapid Commun*. 43 (2022).
601 <https://doi.org/10.1002/MARC.202100585>.
- 602 [21] T. Luo, S. Lin, R. Xie, X.J. Ju, Z. Liu, W. Wang, C.L. Mou, C. Zhao, Q. Chen, L.Y. Chu, pH-
603 responsive poly(ether sulfone) composite membranes blended with amphiphilic polystyrene-
604 block-poly(acrylic acid) copolymers, *Journal of Membrane Science*. 450 (2014) 162–173.
605 <https://doi.org/10.1016/J.MEMSCI.2013.09.002>.
- 606 [22] H. Salehi, A. Shakeri, H. Mahdavi, R.G.H. Lammertink, Improved performance of thin-film
607 composite forward osmosis membrane with click modified polysulfone substrate,
608 *Desalination*. (2020). <https://doi.org/10.1016/j.desal.2020.114731>.
- 609 [23] M.G. Kochameshki, M. Mahmoudian, A. Marjani, K. Farhadi, M. Enayati, H.S. Mollayousefi,
610 Graphene oxide grafted poly(acrylic acid) synthesized via surface initiated RAFT as a pH-
611 responsive additive for mixed matrix membrane, *Journal of Applied Polymer Science*. (2019).
612 <https://doi.org/10.1002/app.47213>.

- 613 [24] X. Deng, J.L. Livingston, N.J. Spear, G.K. Jennings, PH-Responsive Copolymer Films Prepared by
614 Surface-Initiated Polymerization and Simple Modification., *Langmuir*. (2020).
615 <https://doi.org/10.1021/acs.langmuir.9b03026>.
- 616 [25] A. Walther, A. Walther, Viewpoint: From Responsive to Adaptive and Interactive Materials
617 and Materials Systems: A Roadmap, *Advanced Materials*. 32 (2020) 1905111.
618 <https://doi.org/10.1002/adma.201905111>.
- 619 [26] T.S. Wong, S.H. Kang, S.K.Y. Tang, E.J. Smythe, B.D. Hatton, A. Grinthal, J. Aizenberg,
620 Bioinspired self-repairing slippery surfaces with pressure-stable omniphobicity, *Nature* 2011
621 477:7365. 477 (2011) 443–447. <https://doi.org/10.1038/nature10447>.
- 622 [27] G.R. Gossweiler, G.B. Hewage, G. Soriano, Q. Wang, G.W. Welshofer, X. Zhao, S.L. Craig,
623 Mechanochemical activation of covalent bonds in polymers with full and repeatable
624 macroscopic shape recovery, *ACS Macro Letters*. 3 (2014) 216–219.
625 https://doi.org/10.1021/MZ500031Q/SUPPL_FILE/MZ500031Q_SI_002.PDF.
- 626 [28] X. Chen, M.A. Dam, K. Ono, A. Mal, H. Shen, S.R. Nutt, K. Sheran, F. Wudl, A thermally re-
627 mendable cross-linked polymeric material, *Science* (1979). 295 (2002) 1698–1702.
628 https://doi.org/10.1126/SCIENCE.1065879/SUPPL_FILE/1065879S3_THUMB.GIF.
- 629 [29] S.R. White, J.S. Moore, N.R. Sottos, B.P. Krull, W.A. Santa Cruz, R.C.R. Gergely, Restoration of
630 large damage volumes in polymers, *Science* (1979). 344 (2014) 620–623.
631 https://doi.org/10.1126/SCIENCE.1251135/SUPPL_FILE/WHITE-SM.PDF.
- 632 [30] C.W. Park, S.K. Kang, H.L. Hernandez, J.A. Kaitz, D.S. Wie, J. Shin, O.P. Lee, N.R. Sottos, J.S.
633 Moore, J.A. Rogers, S.R. White, Thermally triggered degradation of transient electronic
634 devices, *Adv Mater*. 27 (2015) 3783–3788. <https://doi.org/10.1002/ADMA.201501180>.
- 635 [31] R. Yoshida, T. Takahashi, T. Yamaguchi, H. Ichijo, Self-Oscillating Gel, *Undefined*. 118 (1996)
636 5134–5135. <https://doi.org/10.1021/JA9602511>.
- 637 [32] S. Maeda, Y. Hara, T. Sakai, R. Yoshida, S. Hashimoto, Self-Walking Gel, *Advanced Materials*.
638 19 (2007) 3480–3484. <https://doi.org/10.1002/ADMA.200700625>.
- 639 [33] R. Yoshida, Y. Murase, Self-oscillating surface of gel for autonomous mass transport, *Colloids
640 and Surfaces B: Biointerfaces*. 99 (2012) 60–66.
641 <https://doi.org/10.1016/J.COLSURFB.2011.09.036>.
- 642 [34] D. Suzuki, T. Kobayashi, R. Yoshida, T. Hirai, Soft actuators of organized self-oscillating
643 microgels, *Soft Matter*. 8 (2012) 11447–11449. <https://doi.org/10.1039/C2SM26477C>.
- 644 [35] T. Sakata, S. Nishitani, Y. Yasuoka, S. Himori, K. Homma, T. Masuda, A.M. Akimoto, K. Sawada,
645 R. Yoshida, Self-oscillating Chemoelectrical Interface of Solution-gated Ion-sensitive Field-
646 effect Transistor Based on Belousov–zhabotinsky Reaction, *Null*. (2021).
647 <https://doi.org/10.21203/rs.3.rs-1110032/v1>.
- 648 [36] T. Yamamoto, R. Yoshida, Self-oscillation of polymer and photo-regulation by introducing
649 photochromic site to induce LCST changes, *Reactive and Functional Polymers*. 73 (2013) 945–
650 950. <https://doi.org/10.1016/J.REACTFUNCTPOLYM.2013.02.015>.
- 651 [37] K. Homma, Y. Ohta, K. Minami, G. Yoshikawa, K. Nagase, A.M. Akimoto, R. Yoshida,
652 Autonomous Nanoscale Chemomechanical Oscillation on the Self-Oscillating Polymer Brush

- 653 Surface by Precise Control of Graft Density., *Langmuir*. (2021).
654 <https://doi.org/10.1021/acs.langmuir.1c00459>.
- 655 [38] T. Geher-Herczegh, Z. Wang, T. Masuda, R. Yoshida, N. Vasudevan, Y. Hayashi, Delayed
656 Mechanical Response to Chemical Kinetics in Self-Oscillating Hydrogels Driven by the
657 Belousov-Zhabotinsky Reaction., *Macromolecules*. (2021).
658 <https://doi.org/10.1021/acs.macromol.1c00402>.
- 659 [39] M. Benoit, D. Bouyer, P. Sizat, A. Ayrat, D. Cot, B. Rebiere, D. Fournier, J. Lyskawa, P. Woisel,
660 C. Antonelli, D. Quemener, Self-Oscillating Membranes with Polymer Interface Synchronized
661 with Chemical Oscillator to Reproduce Lifelike Pulsatile Flow, *Chemistry of Materials*. 33
662 (2021) 998–1005. <https://doi.org/10.1021/acs.chemmater.0c04009>.
- 663 [40] M.R. Whittaker, Y.K. Goh, H. Gemici, T.M. Legge, S. Perrier, M.J. Monteiro, Synthesis of
664 Monocyclic and Linear Polystyrene Using the Reversible Coupling/Cleavage of Thiol/Disulfide
665 Groups, *Macromolecules*. 39 (2006) 9028–9034. <https://doi.org/10.1021/MA061070E>.
- 666 [41] E. Cazares-Cortes, B.C. Baker, K. Nishimori, M. Ouchi, F. Tournilhac, Polymethacrylic Acid
667 Shows Thermoresponsivity in an Organic Solvent, *Macromolecules*. 52 (2019) 5995–6004.
668 <https://doi.org/10.1021/acs.macromol.9b00412>.
- 669 [42] I. Lacík, M. Stach, P. Kasák, V. Semak, L. Uhelská, A. Chovancová, G. Reinhold, P. Kilz, G.
670 Delaittre, B. Charleux, I. Chaduc, F. D’Agosto, M. Lansalot, M. Gaborieau, P. Castignolles, R.G.
671 Gilbert, Z. Szablan, C. Barner-Kowollik, P. Hesse, M. Buback, SEC Analysis of Poly(Acrylic Acid)
672 and Poly(Methacrylic Acid), *Macromolecular Chemistry and Physics*. 216 (2015) 23–37.
673 <https://doi.org/10.1002/MACP.201400339>.
- 674 [43] H. Lee, S.M. Dellatore, W.M. Miller, P.B. Messersmith, Mussel-inspired surface chemistry for
675 multifunctional coatings, *Science* (1979). 318 (2007) 426–430.
676 https://doi.org/10.1126/SCIENCE.1147241/SUPPL_FILE/LEE.SOM.PDF.
- 677 [44] M. Gu, J. Zhang, X. Wang, H. Tao, L. Ge, Formation of poly(vinylidene fluoride) (PVDF)
678 membranes via thermally induced phase separation, *Desalination*. 192 (2006) 160–167.
679 <https://doi.org/10.1016/J.DESAL.2005.10.015>.
- 680 [45] Y. Chen, X. Feng, Y. Zhao, X. Zhao, X. Zhang, Mussel-Inspired Polydopamine Coating Enhances
681 the Intracutaneous Drug Delivery from Nanostructured Lipid Carriers Dependently on a
682 Follicular Pathway, *Molecular Pharmaceutics*. 17 (2020) 1215–1225.
683 https://doi.org/10.1021/ACS.MOLPHARMACEUT.9B01240/SUPPL_FILE/MP9B01240_SI_001.PDF.
- 684 DF.
- 685 [46] H. Sadegh, R. Sahay, S. Soni, Protein–polymer interaction: Transfer loading at interfacial
686 region of PES-based membrane and BSA, *Undefined*. 136 (2019).
687 <https://doi.org/10.1002/APP.47931>.
- 688 [47] F. Schacher, M. Ulbricht, A.H.E. Müller, Self-Supporting, Double Stimuli-Responsive Porous
689 Membranes From Polystyrene-block-poly(N,N-dimethylaminoethyl methacrylate) Diblock
690 Copolymers, *Advanced Functional Materials*. 19 (2009) 1040–1045.
- 691 [48] R.I. Peinador, J.I. Calvo, K. ToVinh, V. Thom, P. Prádanos, A. Hernández, Liquid-liquid
692 displacement porosimetry for the characterization of virus retentive membranes,
693 *Journal of Membrane Science*. 372 (2011) 366–372.
694 <https://doi.org/10.1016/J.MEMSCI.2011.02.022>.

Graphical Abstract

